Biochemical and Biophysical Research Communications 641 (2023) 123–131

Contents lists available at ScienceDirect

Biochemical and Biophysical Research Communications

journal homepage: www.elsevier.com/locate/ybbrc

CCL20/CCR6 chemokine signaling is not essential for pathogenesis in an experimental autoimmune encephalomyelitis mouse model of multiple sclerosis

Nozomi Sachi [a], Naganori Kamiyama [a], Benjawan Saechue [a], Sotaro Ozaka [a], Astri Dewayani [a], Shimpei Ariki [a], Thanyakorn Chalalai [a], Yasuhiro Soga [a], Chiaki Fukuda [a], Yomei Kagoshima [a], Supanuch Ekronarongchai [a], Takashi Kobayashi [a, b, *]

[a] Department of Infectious Disease Control, Faculty of Medicine, Japan
[b] Research Center for GLOBAL and LOCAL Infectious Diseases, Oita University, Oita, Japan

ARTICLE INFO

Article history:
Received 22 November 2022
Accepted 27 November 2022
Available online 30 November 2022

Keywords:
Multiple sclerosis
CCL20
CCR6
Experimental autoimmune encephalomyelitis (EAE)
Autoimmune disease

ABSTRACT

Multiple sclerosis is an autoimmune disease in which the immune system attacks the nerve myelin sheath. The balance between pathogenic Th17 cells and regulatory Treg cells, both of which express the chemokine receptor CCR6 is critical for determining disease activity. It has been postulated that CCL20, the cognate ligand of CCR6, produced by the blood-brain barrier attracts these immune cells to the central nervous system (CNS). However, the pathological phenotypes of the experimental model of multiple sclerosis in CCR6-knockout (KO) mice are inconclusive, while this has not been addressed in CCL20-KO mice.

To address this, we generated CCL20-KO and CCR6-KO mice using the CRISPR/Cas9 system. Clinical phenotypes of experimental autoimmune encephalomyelitis (EAE) in the chronic phase were slightly exacerbated in both mutant mice relative to those in wild-type (WT) mice. Inflammatory cell infiltration and demyelination in the CNS were similar in the KO and WT mice. CNS $CD4^+$ T cell counts were the same for mutant and WT mice. The mutant and WT mice did not differ significantly in the proportions of Th17 and Treg cells in the CNS, or in IL-17 and TGF-β mRNA expression in the CNS.

These findings suggest that CCL20/CCR6-mediated cell migration is not necessarily required for the onset of EAE, and may be compensated for by other chemokine signals.

1. Introduction

Chemokines are chemotactic cytokines that regulate immune cell migration. Immune cells expressing the cognate chemokine receptor migrate to the site of inflammation in response to gradients of the respective ligands. Thus, chemokines and their receptors play key roles in the homeostasis and pathogenesis of various diseases, including tumors, infectious diseases, and autoimmune diseases [1]. In the CC class of chemokines, 28 members (CCL1–CCL28) bind to their cognate CC chemokine receptors (CCR1–CCR10) which are expressed predominantly by T cells, monocytes, macrophages, and dendritic cells (DCs) [1]. Most chemokines bind to and activate multiple receptors, whereas a single chemokine receptor is associated with several chemokine ligands [1]. This overlapping ligand–receptor specificity makes it difficult to elucidate the biological functions of each ligand or receptor.

CCL20, also known as macrophage inflammatory protein (MIP)-3α, induces migration via its cognate receptor, CCR6 [2]. The basal expression of CCL20 is limited to the skin and mucosal surfaces, and is further increased in response to inflammatory agents such as PMA, ionomycin, TNF-α, and LPS [3–6]. Recently, it has been postulated that astrocytes that form the blood-brain barrier produce CCL20, which in turn allows CCR6-expressing immune cells to infiltrate the central nervous system (CNS). CCL20 expression in astrocytes has been shown to be induced by IL-6 combined with IL-17, and RANKL [7,8]. Inflammation in the CNS is highly associated with neurodegenerative diseases such as multiple sclerosis (MS), in

* Corresponding author. Department of Infectious Disease Control, Faculty of Medicine, Oita University, 1-1 Idaigaoka, Hasama, Yufu, Oita, 879-5593, Japan.
E-mail address: takashik@oita-u.ac.jp (T. Kobayashi).

https://doi.org/10.1016/j.bbrc.2022.11.088
0006-291X/

which $CD4^+$ T helper (Th) cells are responsible for coordinating the activation and suppression of the host immune response in the disease. For instance, Th17 cells shape the pathogenesis of MS, whereas Treg cells suppress the disease [9]. Both T cell subsets highly express the chemokine receptor CCR6, and are attracted to CCL20 in target tissues [1].

CCL20 and CCR6 are unique in that they interact only with each other [1]. Targeted disruption of CCL20 or CCR6 in mice is therefore expected to produce a distinct phenotype associated with immune cell migration and inflammatory responses. However, the pathological role of CCL20 in experimental autoimmune encephalomyelitis (EAE), a model of MS, has not been assessed using CCL20-knoockout (KO) mice. Moreover, the pathological phenotypes of EAE in CCR6-KO mice generated by embryonic stem (ES) cell-mediated homologous recombination were not consistent between the research groups. For example, some groups have reported that CCR6-KO mice exhibit more severe EAE [10,11], while others have reported mild EAE [12–14]. These phenotypic differences between studies, following EAE induction, may be due to the heterogeneity of the genetic backgrounds of the mutant mice used.

In this study, we generated CCL20-KO and CCR6-KO mice with a C57BL/6 genetic background using the CRISPR/Cas9 system, examining the pathological scores and body weight loss of the mutant and wild-type mice, and using histopathological staining to investigate inflammatory cell infiltration and demyelination in the CNS. Flow cytometry was used to compare CNS $CD4^+$ T cell counts. Th17 and Treg cell counts, and IL-17 and TGF-β mRNA expression levels in the CNS, were examined.

2. Materials and methods

2.1. Mice

C57BL/6 mice were purchased from Japan SLC (Hamamatsu, Japan). The CCL20 and CCR6 target sequences of the gRNA are shown in Fig. 1 gRNA and Cas9 were purchased from Integrated DNA Technologies, Inc. (Coralville, IA, USA). Genome editing of fertilized eggs in the oviduct (i-GONAD) was performed as described [15]. Briefly, on the day after mating, gRNA and Cas9 were injected into the ampulla of the oviducts of C57BL/6 female mice with confirmed plugs. Electrodes were then placed between the oviducts and pulses were applied using a NEPA21 Electroporator (NEPA GENE Co. Ltd., Chiba, Japan). The mice were maintained in a specific pathogen-free facility in the Division of Laboratory Animal Science at Oita University. All experimental protocols were approved by the Oita University Animal Ethics Committee (approval number 170902).

2.2. Experimental autoimmune encephalomyelitis (EAE) induction and disease scoring

To induce EAE, each mouse was immunized s.c. on day 0 with 160 μg myelin oligodendrocyte glycoprotein (MOG) peptide (aa 35–55) (MEVGWYRSPFSRVVHLYRNGK) (SynPeptide Co. Ltd., Shanghai, China), emulsified in CFA supplemented with 2.2 mg/ml *Mycobacterium tuberculosis*, and was injected i.p. on days 0 and 2 with 400 ng pertussis toxin (List Biological Laboratories, Inc. Campbell, CA), as described [16]. The following clinical scoring system was used: 0, no disease; 1, reduced tail tonus; 2, tail limpness; 3, ataxia; 4, paralyzed hind limbs; 5, quadriplegia; and 6, death. Scoring was performed every 24 h.

2.3. Histological evaluation

After disease induction, the mice were euthanized by cervical dislocation. The brains and spinal cords were obtained and fixed in 10% formalin for 48 h. Paraffin-embedded tissue samples were sectioned and stained with hematoxylin–eosin (HE) and Luxol Fast Blue (LFB) to identify cellular infiltration and demyelination, respectively.

2.4. Flow cytometry

Fluorochrome-conjugated antibodies against CD3, CD4, CD8α, CD11c, PD-L1, CCR6, IL-17, and IFN-γ were purchased from BioLegend (San Diego, CA, USA). Antibodies against CD4, CD11b, CD44, B220, IgM, IgD, and Foxp3 were purchased from BD Biosciences (Franklin Lakes, NJ, USA) and F4/80, CD25, CD3, and CD8α were purchased from eBiosciences (Santa Clara, CA, USA). Total cells from the spleen, thymus, bone marrow, brain, and spinal cord were stained with antibodies against cell-surface molecules for 20 min. In some experiments, cells were fixed and permeabilized using an IC fixation/permeabilization kit from e-Bioscience (San Diego, CA) for intracellular staining (ICS). ICS was performed according to the manufacturer's protocol using anti-IFN-γ-FITC, anti-IL-17-PE, and anti-Foxp3-APC. Flow cytometric analysis was performed on a FACS LSR Fortessa X-20 flow cytometer (BD Biosciences) using FlowJo (Tree Star).

2.5. ELISA

CCL20 protein concentration was determined using the mouse CCL20/MIP-3 alpha DuoSet (R&D Systems, Minneapolis, MN, USA), according to the manufacturer's protocol. OD at 450 nm was determined using a Model 680 microplate reader (Bio-Rad, Hercules, CA, USA).

2.6. Quantitative real-time RT-PCR

Total RNA was extracted using TRI Reagent1 (Sigma-Aldrich), purified using a PureLink RNA Mini Kit (Thermo Fisher Scientific Inc., Waltham, MA, USA), and then reverse-transcribed using a Verso cDNA Synthesis Kit (Thermo Fisher Scientific Inc.). Quantitative RT-PCR was performed using a real-time PCR machine (LightCycler 96, Roche Diagnostics, Rotkreuz, Switzerland) with a KAPA SYBR FAST qPCR Kit (Kapa Biosystems, Wilmington, MA, USA). Relative mRNA levels were normalized to those of β-actin, and all data were analyzed using LightCycler Software 1.1 (Roche Diagnostics). The primer sequences are listed in Supplementary Table S1.

2.7. Immunohistochemistry

Spleen samples were freshly frozen in Tissue-Tek OCT compound (Sakura Finetek, Tokyo, Japan) and cut into slices 10 μm thick using a Leica CM3050 S Cryostat (Wetzlar, Germany). The frozen sections were stained with anti-CD3-APC, anti-B220-PE, and anti-CD169-FITC (BioLegend). Images were captured with a BZ-9000 Biorevo All-in-one Fluorescence Microscope (KEYENCE Corporation, Osaka, Japan).

2.8. Statistical analysis

All data are presented as the mean ± SEM. Univariate analysis between two groups was performed with the Mann-Whitney *U* test using GraphPad Prism7 (GraphPad Software, San Diego, CA, USA). $P < 0.05$ was considered statistically significant.

3. Results

3.1. Establishment of CCL20-KO and CCR6-KO mice

To assess the pathological significance of CCL20 in EAE, CCL20-KO and CCR6-KO mice were generated using the CRISPR/Cas9

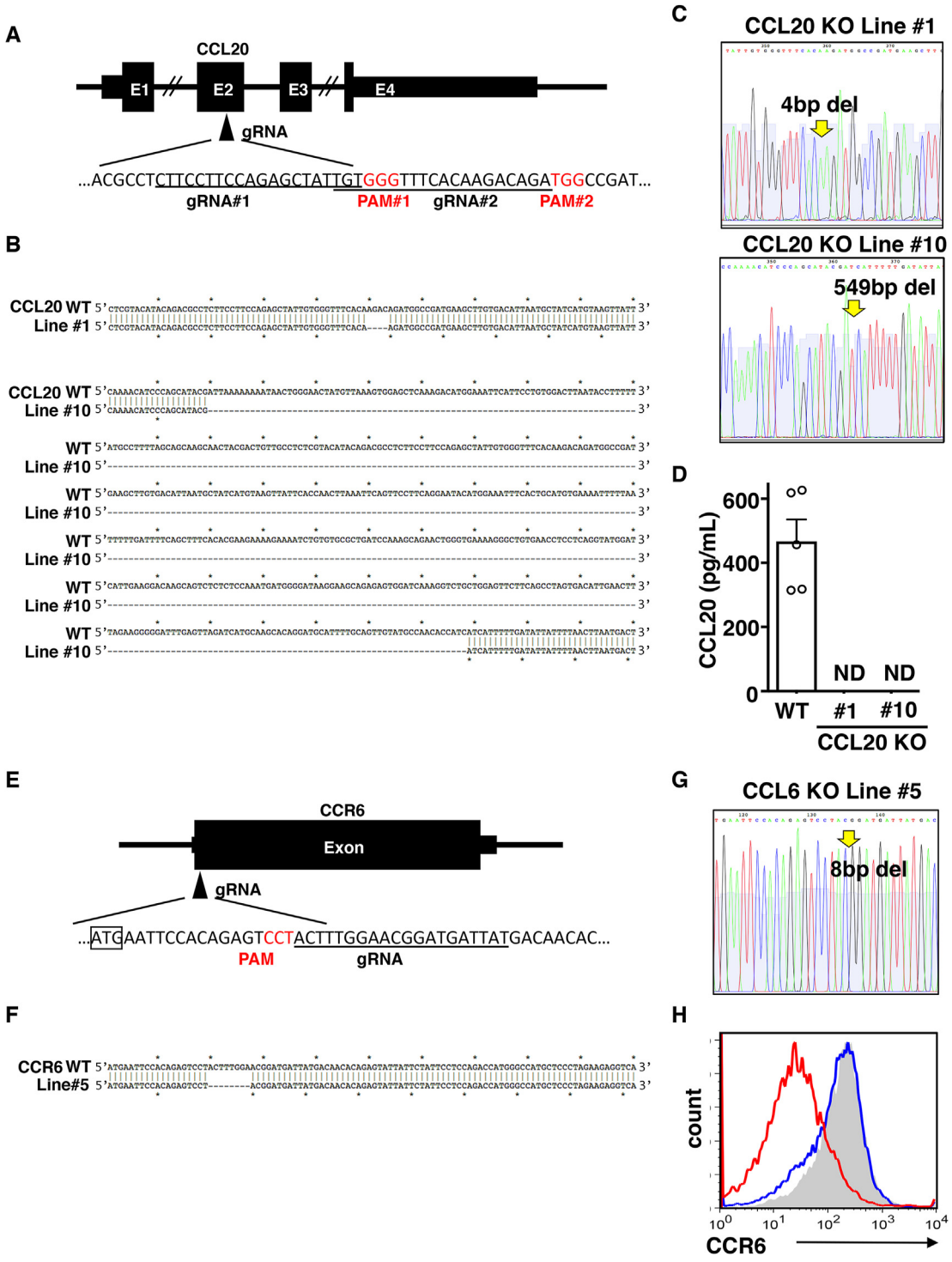

Fig. 1. CRISPR/Cas9-mediated deletion of murine CCL20 and CCR6 genes.
(**A**) Gene structure of *CCL20* with CRISPR/Cas9 target sites. Two gRNA target sequences in exon2 of *CCL20* are underlined. Red letters represent the PAM (protospacer adjacent motif). (**B**) Sequence alignment confirming deletions of 4 bp and 549 bp in *CCL20*, in mutant lines 1 and 10, respectively. (**C**) Representative sequencing chromatograms of the homozygous *CCL20* mutant in lines 1 and 10. Arrows indicate mutation sites. (**D**) CCL20 protein levels in the Peyer's patches (PP). ELISA of CCL20 expression in wild-type (WT) and CCL20-KO mice (lines 1 and 10). ND: not detected. (**E**) *CCR6* gene structure, with the CRISPR/Cas9 target site. The RNA target sequence in the *CCR6* gene is underlined. The sequence in the box represents the first codon of *CCR6*. (**F**) Sequence alignment confirming an 8 bp deletion in *CCR6* (line 5). (**G**) Representative sequencing chromatograms of the edited *CCR6* gene in line 5. Arrow indicates the mutation site. (**H**) CCR6 protein levels on splenic B cells from WT (shaded), CCL20-KO (blue) and CCR6-KO (red) mice, via flow cytometry. . (For interpretation of the references to colour in this figure legend, the reader is referred to the Web version of this article).

system. We designed two gRNAs targeting exon 2 of murine CCL20, and injected them along with Cas9 protein directly into the ampulla of the oviducts of C57BL/6 plugged female mice (Fig. 1A), followed by in vivo electroporation using an NEPA21 Electroporator (NEPA GENE Co. Ltd., Chiba, Japan) [15]. Sequencing analysis revealed several mutations in CCL20 exon 2. Mice with deletions of 4 bp or 549 bp in exon 2 (hereafter, lines 1 and 10) were selected for further experiments (Fig. 1B). Mice heterozygous for these CCL20

mutations were intercrossed to generate homozygous (CCL20-KO) offspring (Fig. 1C). ELISA-based confirmation of CCL20 protein levels in the Peyer's patches (PP) revealed that CCL20 protein expression was abolished in CCL20-KO lines 1 and 10 (Fig. 1D).

To examine the EAE-induced phenotype in CCR6-KO mice, we generated CCR6-KO mice using CRISPR/Cas9-mediated gene deletion in syngeneic C57BL/6 mice. We designed a gRNA targeting the first coding exon of CCR6 (Fig. 1E) and obtained founder mice carrying an 8 bp deletion in CCR6 (Fig. 1F). Mice heterozygous for this CCR6 mutation were intercrossed to generate homozygous (CCR6-KO) offspring (Fig. 1G). Flow cytometric analysis confirmed the lack of CCR6 protein expression on the surface of B cells in CCR6-KO mice, but not in wild-type or CCL20-KO mice (Fig. 1H). Both CCL20-KO and CCR6-KO mice were born at a normal Mendelian ratio.

3.2. Normal leukocyte populations in lymphoid organs of CCL20-KO and CCR6-KO mice

T cell development occurs in distinct compartments of the thymus, and involves intrathymic thymocyte migration regulated by chemokines [17]. To examine whether the CCL20/CCR6 axis regulates this migration, we analyzed thymic cell populations using flow cytometry. The proportions of double-negative (DN), double-positive (DP), CD4 single-positive (SP) and CD8 SP subsets were equivalent (Fig. 2A), with no significant differences in the proportions of these subsets among the three groups (Fig. 2B). Moreover, the DN1 ($CD25^{-}CD44^{+}$), DN2 ($CD25^{+}CD44^{+}$), DN3 ($CD25^{+}CD44^{-}$), and DN4 ($CD25^{-}CD44^{-}$) populations in the DN subset were comparable among the three groups (Fig. 2C and D). Analysis of B cell development in the bone marrow revealed that the ratios of the Pro-/Pre-B cell population ($B220^{int}IgM^{-}IgD^{-}$), immature B cell population ($B220^{int}IgM^{+}IgD^{-}$), and recirculating B cell population ($B220^{high}IgM^{+}IgD^{+}$) were normal in CCL20-KO and CCR6-KO mice (Fig. 2E). These data suggest that the CCL20/CCR6 axis is not required for normal lymphocyte development in the thymus and bone marrow.

Next, we examined the splenic architecture and cell populations. Splenic weight and cellularity were comparable among the three genotypes (Fig. 3A and B). Immunohistochemical (IHC) analysis of spleen sections revealed that CCL20-KO and CCR6-KO mice showed normal splenic architecture, in which typical T cell areas were surrounded by follicular and marginal-zone B cell areas separated by marginal zone macrophages (Fig. 3C). Moreover, flow cytometric analysis revealed that splenic $B220^{+}$ B cells, $CD3^{+}$ T cell frequencies, and CD4/CD8 ratios in $CD3^{+}$ T cell populations were comparable among the three groups (Fig. 3D–G). The frequencies of $CD11c^{+}$ dendritic cells (DCs) and $CD11b^{+}$ macrophages were essentially equivalent among the groups (Fig. 3H and I). These data suggest that the CCL20/CCR6 axis is not necessary to maintain normal splenic architecture and cell populations.

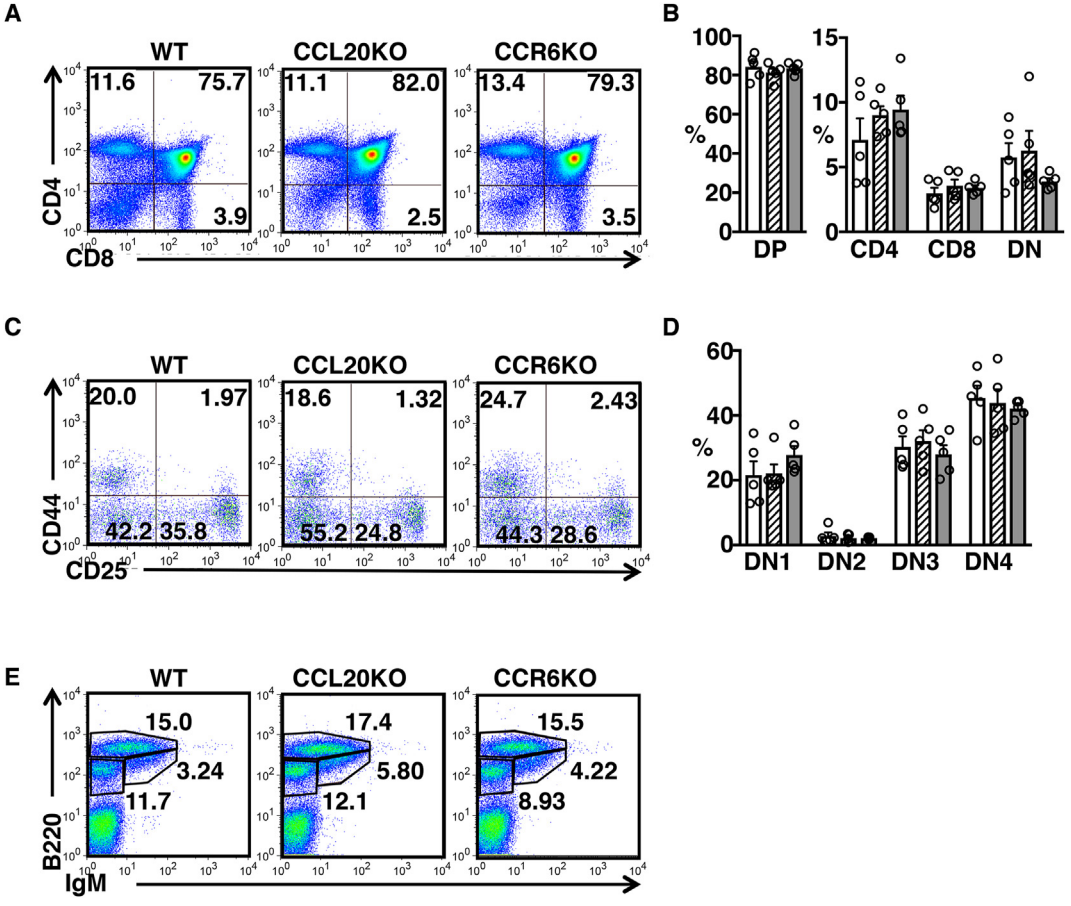

Fig. 2. Flow cytometry of leukocytes in the thymus and bone marrow.
(**A**–**D**). Thymocytes from wild-type (WT), CCL20-knockout (CCL20-KO), and CCR6-KO mice, stained with fluorochrome-conjugated antibodies. (**A**) Representative flow cytometry using anti-CD4 and anti-CD8α antibodies for DN, DP, CD4, and CD8 SP cells. (**B**) Percentages of T cell subsets in WT (open bar), CCL20-KO (hatched bar), and CCR6-KO (gray bar) mice. Representative flow cytometry, using anti-CD25 and anti-CD44 antibodies, for subsets DN1–DN4 subsets (**C**), and percentages of DN subsets (n = 5) (**D**). (**E**) Bone marrow cells stained with anti-B220 and anti-IgM antibodies. Numbers in the dot plots denote cells in the gate as a percentage of the parent population. Data are representative of three independent experiments.

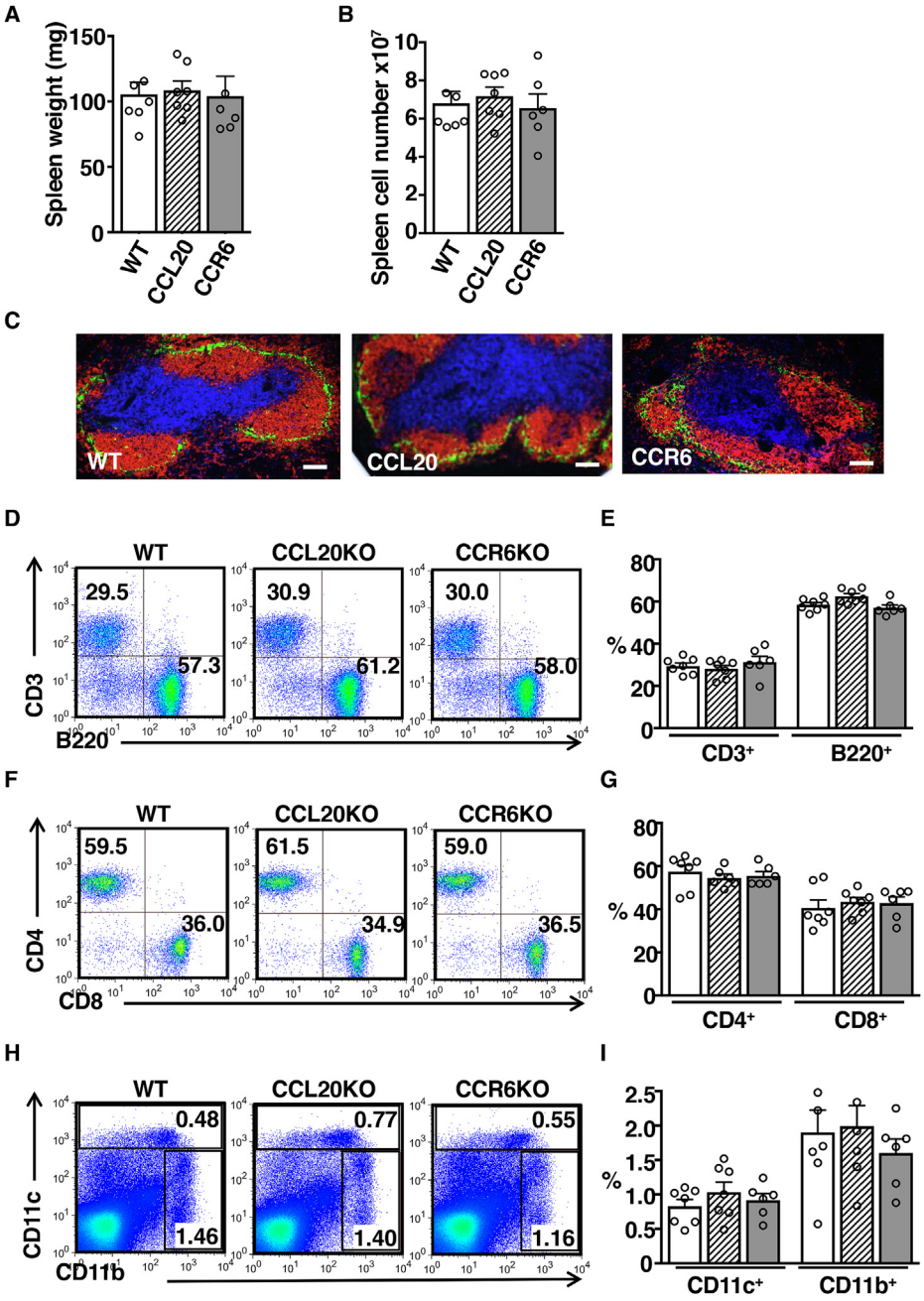

Fig. 3. Flow cytometry of leukocytes in the spleen.
Weights (**A**) and total cell numbers (**B**) in the spleens of wild-type (WT), CCL20-deficient (CCL20), and CCR6-deficient (CCR6) mice (n > 6). (**C**) Splenic microarchitecture was visualized via immunohistochemical staining with anti-B220 (red), anti-CD3 (blue), and anti-CD169 (green) antibodies. Results are representative of at least three mice. Scale bars represent 100 μm. (**D**–**I**) Splenocytes were stained with the indicated antibodies and analyzed via flow cytometry. (**D**) Cells stained with anti-B220 and anti-CD3 antibodies for B and T cells. (**E**) Percentages of $CD3^+$ T cell and $B220^+$ B cells in the spleens of WT (open bar), CCL20-KO (hatched bar), and CCR6-KO (gray bar) mice. (**F**) CD4 and CD8 expression in $CD3^+$ cells. (**G**) Percentages of $CD4^+$ and $CD8^+$ T cell subsets of $CD3^+$ T cells in the spleen. (**H**) Splenocytes stained with anti-CD11b and anti-CD11c. (**I**) Percentages of $CD11c^+$ DC and $CD11b^+$ macrophages in the spleen. Numbers in the dot plots denote cells in the gate as a percentage of the parent population. Data are representative of three independent experiments. . (For interpretation of the references to colour in this figure legend, the reader is referred to the Web version of this article).

3.3. EAE development in CCL20-KO and CCR6-KO mice

Although some studies have shown that CCR6-KO mice with EAE exhibit less CNS pathology [12–14], others have reported that CCR6-KO mice exhibit exacerbated EAE [10. 11]. Kohler et al. showed that treatment with anti-CCL20 antibody significantly reduced the severity of EAE by inhibiting the sensitization of peripheral T cells [18]. To clarify the pathological role of the CCL20/CCR6 axis in EAE, we induced EAE in WT, CCL20-KO, and CCR6-KO mice with a C57BL/6 genetic background, via MOG_{35-55} immunization.

The MOG_{35-55}-immunized mice all displayed prominent body weight loss, beginning ca. 10–12 d post immunization (dpi) (Fig. 4A). In WT mice, the maximum weight loss was at ca. 14 dpi, followed by recovery over 5 d. However, both CCL20-KO and CCR6-KO mice showed delayed recovery of body weight during the recovery phase of EAE. The clinical score in EAE-induced mice peaked at 3.0 ± 0.0 (for WT), 3.4 ± 0.2 (for CCL20-KO), and 4.0 ± 0.0 (for CCR6-KO). Shortly after peaking, WT mice showed a partial reduction in EAE symptoms (Fig. 4B). However, most of the CCL20-KO and CCR6-KO mice exhibited sustained severe paralytic disease

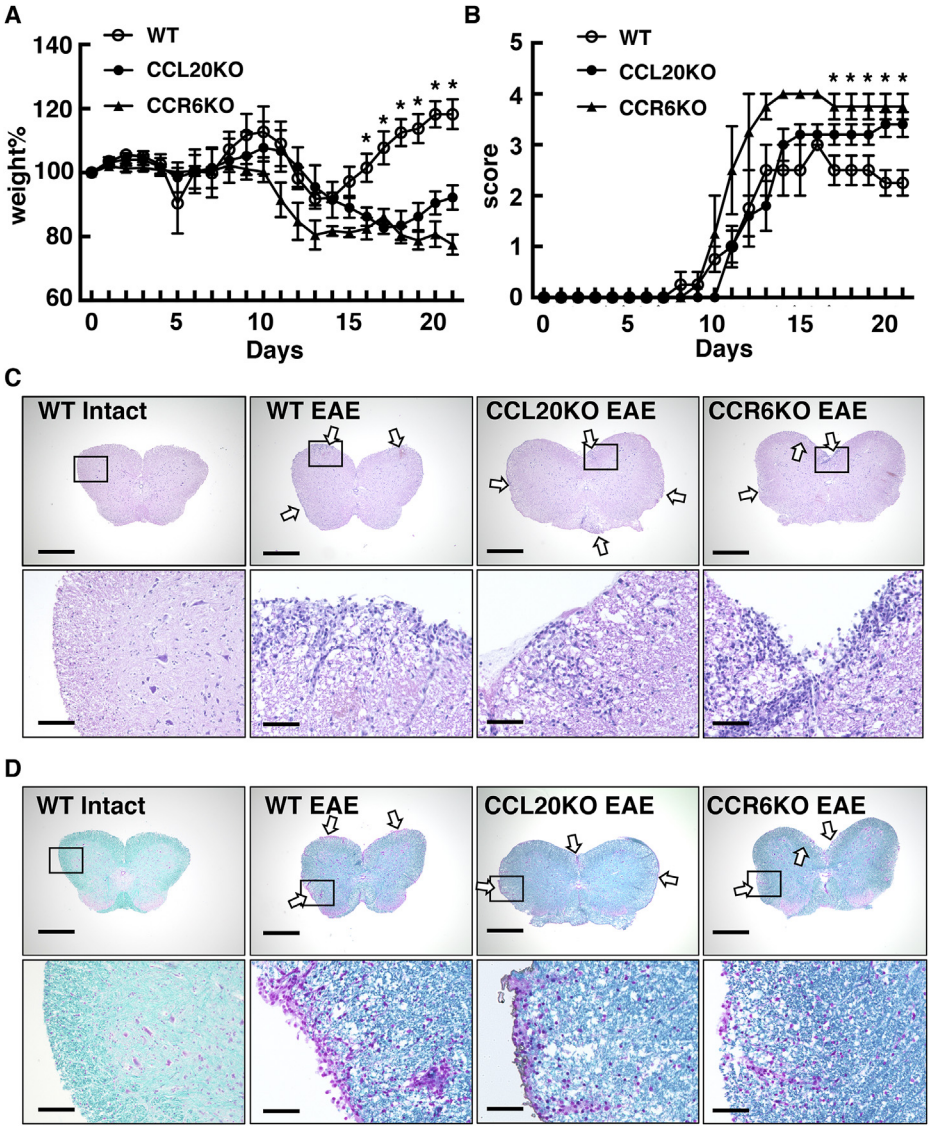

Fig. 4. Increased disease severity and delayed recovery of experimental autoimmune encephalomyelitis (EAE) in CCL20-knockout (KO) and CCR6-KO mice.
Wild-type (open circles; n = 5), CCL20-deficient (closed circles; n = 5), and CCR6-deficient (closed triangles; n = 5) mice on a C57BL/6 background, immunized with MOG_{35-55} emulsified in CFA, and monitored for body weight (**A**) and clinical scores of EAE (**B**). Data are representative of at least three independent experiments. *, $P < 0.05$. (**C**) Immune cell infiltration in the spinal cord was evaluated via HE-staining. Representative images of coronal sections of the spinal cord in mice with MOG-induced EAE (21 d post-immunization [dpi]) are shown in the upper panels. Arrows indicate infiltration of inflammatory cells. Higher-magnification images of the rectangle in the upper panels are shown in the lower panels. Scale bars represent 600 μm (upper) and 100 μm (lower). (**D**) Demyelination in the spinal cord was evaluated using LFB staining at 21 dpi. The demyelinated areas are indicated by the arrows. Higher-magnification images of the rectangle in the upper panels are shown in the lower panels. Scale bars represent 600 μm (upper) and 100 μm (lower).

until the end of the experiment. Based on HE-staining, the extent of mononuclear cell infiltration in the spinal cord was comparable among the three groups of EAE mice (Fig. 4C), as was the extent of demyelination, evaluated via LFB staining (Fig. 4D). These results indicate that the absence of the CCL20/CCR6 axis has less impact on the clinical outcomes of EAE in the mutant mice generated using CRISPR/Cas9-mediated genome editing than in those generated using ES cell-mediated gene targeting.

3.4. Infiltration of Th17 and Treg cells into the CNS in CCL20-KO and CCR6-KO mice

To understand the underlying causes of EAE development in CCL20-KO and CCR6-KO mice, cell infiltration and cytokine production in the CNS were analyzed. The absolute numbers of $CD4^+$ cells in the brains of EAE mice were comparable among the three genotypes (Fig. 5A). When we analyzed the frequency of distinct helper T cell subsets such as Th17, Treg, and Th1 cells via flow cytometry, the ratio of IL-17^+, $Foxp3^+$, and IFN-γ^+ cells to $CD4^+$ T cells in the brain was statistically comparable among the three groups (Fig. 5B and C, Supp. Figs. S1A and B). The three groups of EAE mice did not differ significantly in mRNA expression of *IL-17A*, *Foxp3*, or *TGF-β* in the spinal cord (Fig. 5D), or in *IFN-γ* and *IL-10* expression in the spinal cord (Supp. Fig. S1C). These results suggest that neither CCL20 nor CCR6 is required for the proper migration of Th17 and Treg cells into the CNS.

Enhanced chronic EAE in CCR6-KO mice is associated with reduced presence of PD-$L1^+$-regulatory DCs in the spleen [11]. We therefore examined the accumulation of regulatory DCs in the spleens of EAE-induced mice at 28 dpi. The frequencies of splenic $CD11c^+$ DCs in the EAE-treated mice were comparable among the three groups (Fig. 6A and B), as were those of splenic $CD11b^+F4/80^+$ macrophages (Fig. 6C and D). Interestingly, DC expression of PD-L1 was elevated in the EAE-induced mutant mice (Fig. 6E): the

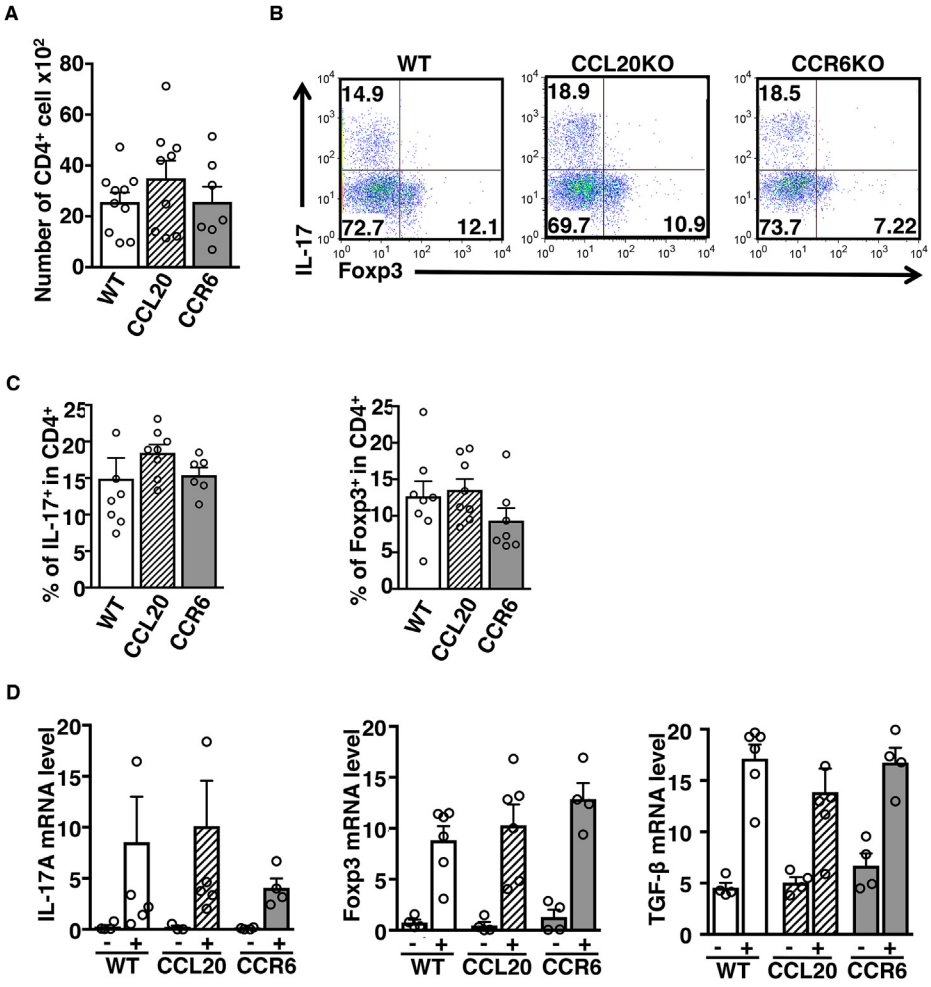

Fig. 5. Comparable frequency of Th17 and Treg cells in the CNS of mice with experimental autoimmune encephalomyelitis (EAE).
(**A**) Mononuclear cells from the brain were prepared from WT (open bar), CCL20-knockout (KO) (hatched bar) and CCR6-KO (gray bar) mice with EAE and stained for CD4. Following staining, the cells were analyzed via flow cytometry, and absolute numbers of $CD4^+$ T cell subsets in the brain were calculated. (**B**) Representative flow cytometry of Th17 and Treg cells in the brain from EAE-induced mice. $CD3^+CD4^+$ cells from the brain were intracellularly stained with anti-IL-17 and anti-Foxp3 antibodies. (**C**) Percentages of Th17 and Treg cells in $CD4^+$ T cells. (**D**) The mRNA expression of *IL-17A*, *Foxp3* and *TGF-β* in the spinal cord of mice unimmunized (−) or immunized with MOG peptide (+), measured via real time PCR. Data were normalized to levels of *β-actin*.

geometric mean of PD-L1 fluorescence intensity was significantly higher in CCL20-KO mice than in WT mice (Fig. 6F).

4. Discussion

The pathophysiological function of CCL20 in autoimmune diseases has not previously been investigated using genetically engineered mouse models of human disease. We therefore used CRISPR/Cas9-mediated CCL20-KO and CCR6-KO mice on a syngenic C57BL/6 background, analyzing two lines of CCL20-KO mice: both lines showed the same phenotype as the CCR6-KO mice. Both the CCL20-and CCR6-deficient mice exhibited normal development of T cells in the thymus (Fig. 2A–D), and of B cells in the bone marrow (Fig. 2E). Although it has been reported that the frequency of DN2 and DN3 cells in the thymus was reduced in CCR6-KO mice generated via ES cell-mediated homologous recombination [19], our findings suggest that thymocyte development is normal in the absence of CCL20 or CCR6 on a syngenic C57BL/6 background. Moreover, the splenic architecture and cell populations were normal in the mutant mice (Fig. 3). These findings suggest that the CCL20/CCR6 axis is not required for normal lymphocyte development or homeostatic distribution in primary and secondary lymphoid organs.

To gain insight into the pathological roles of the CCL20/CCR6 axis in autoimmune diseases, we compared the clinical phenotypes of EAE in CCL20-KO, CCR6-KO, and WT mice. The two mutant lines exhibited slightly but significantly worse body weight loss and clinical scores than the WT mice (Fig. 4A and B). Histological analysis revealed that inflammatory cell infiltration and demyelination in the CNS were comparable among the three groups (Fig. 4C and D). Previously, three independent groups reported that ES cell-derived CCR6-KO mice are resistant to EAE induction, due to impaired recruitment of helper T cells, including Th17 and Treg cells, into the CNS [12–14] However, we observed comparable numbers of $CD4^+$ T cells in the brains of EAE-induced CCL20-KO, CCR6-KO, and WT mice (Fig. 5A). In addition, the frequencies of Th17, Treg, and Th1 cells in the CNS, as determined via flow cytometry and real-time PCR, were comparable among the three groups (Fig. 5B–D, Supp. Fig. S1). In contrast, two independent groups have demonstrated that CCR6-KO mice show exacerbated EAE [10,11]. One possible mechanism of severe EAE in CCR6-KO mice is the reduced frequency of $Foxp3^+$ T cells in the CNS [10]; however, we did not observe any differences in the frequency of $Foxp3^+$ T cells in the CNS (Fig. 5 B-D). Another possible mechanism,

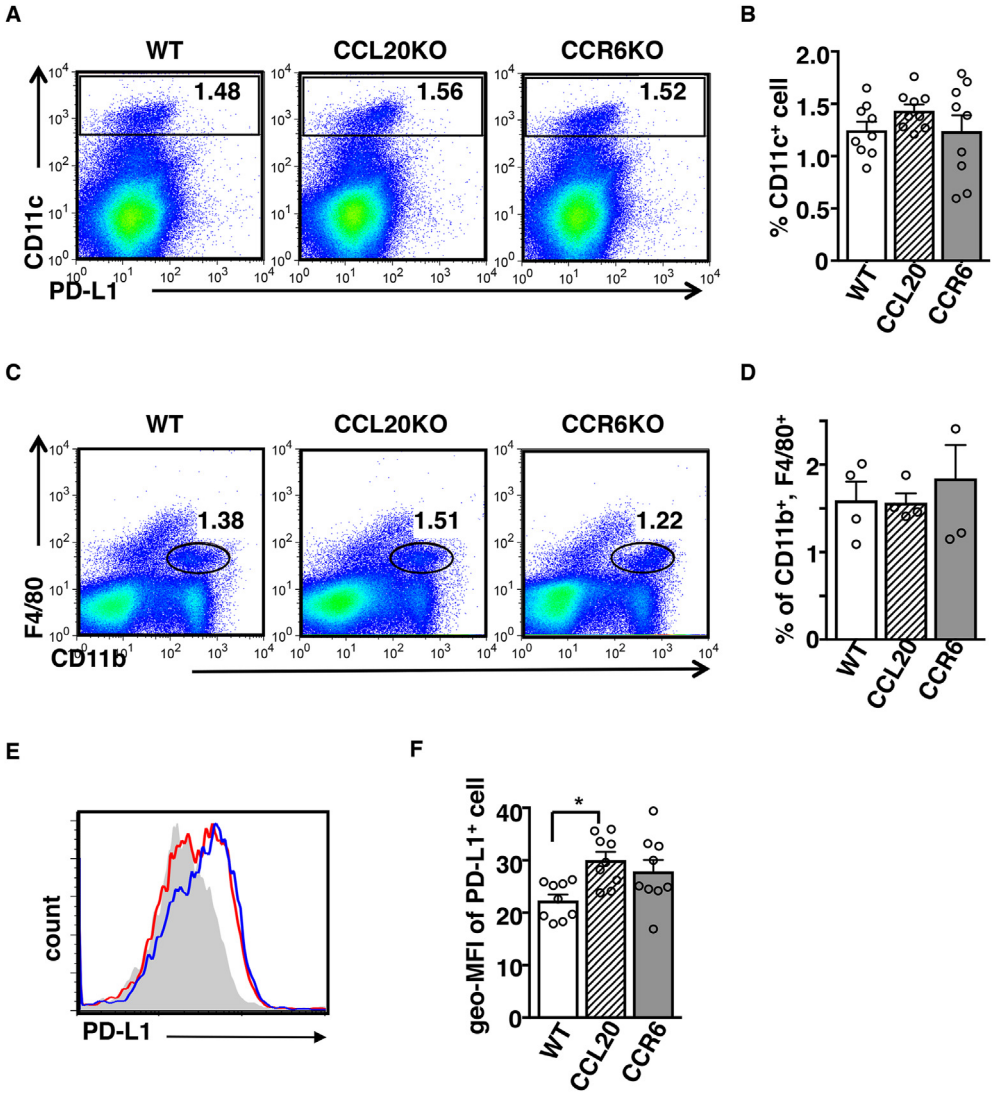

Fig. 6. Relative frequency of dendritic cells (DCs) with increased levels of PD-L1 in the spleens of CCL20-knockout (KO) and CCR6-KO mice with experimental autoimmune encephalomyelitis (EAE).
(**A**) Splenocytes from EAE-induced mice at 28 d post immunization (dpi) were stained for CD11c and PD-L1 and measured via flow cytometry. (**B**) Percentages of $CD11c^+$ DCs. (**C**) Representative data of CD11b and F4/80 staining. (**D**) Percentages of $CD11b^+$ $F4/80^+$ macrophages. (**E**) PD-L1 expression on $CD11c^+$ DC from wild-type (shaded), CCL20-KO (blue), and CCR6-KO (red) mice. (**F**) PD-L1 geometrical mean fluorescence intensity (geo-MFI) on $CD11c^+$ DCs. *, $P < 0.05$. . (For interpretation of the references to colour in this figure legend, the reader is referred to the Web version of this article).

suggested by another group, is a significant reduction in PD-L1-expressing myeloid DCs in the spleen of EAE-induced CCR6-KO mice [11]. In contrast, the frequencies of PD-$L1^+$ $CD11c^+$ myeloid DCs in the spleen were comparable among CCL20-KO, CCR6-KO, and WT mice 28 d after immunization with MOG peptide. PD-L1 geometrical mean fluorescence intensity on DCs was significantly higher in CCL20-KO mice than in WT mice (Fig. 6E and F), suggesting that PD-$L1^+$ regulatory DCs are not responsible for the aggravated clinical phenotypes of EAE in CCL20 and CCR6-KO mice. Previously reported pathological phenotypes of EAE in CCR6-KO mice are not consistent among research groups, probably due to the heterogeneous genetic background of the mutant mice generated via ES cell-mediated homologous recombination. In contrast, we utilized CCL20-KO and CCR6-KO mice generated via CRISPR/Cas9-mediated gene deletion in the syngeneic C57BL/6 strain, which is expected to have a stable phenotype.

Treatment of mice with specific neutralizing anti-CCL20 antibodies significantly reduces the severity of both clinical EAE and neuroinflammation [18]. Our findings, however, do not correspond to this. This contrasting result suggests that neutralizing anti-CCL20 antibodies may inhibit not only CCL20, but also other chemokines.

These findings demonstrate that cell migration via the CCL20/CCR6 axis is not necessarily required for the onset of EAE, and may be compensated for by other chemokine signals. Further investigations are needed to elucidate the molecular regulation of EAE pathogenesis via chemokine signaling in autoimmune diseases.

Declaration of competing interest

The authors have no competing financial interest to declare in relation to the content of this article.

Acknowledgments

We are grateful to Chiharu Aoki, Aiko Yasuda and Shuji Imi for

technical support. We would like to thank Editage (www.editage.com) for English language editing. This work was supported by a grant from the Oita University President's Strategic Discretionary Fund to N.K., S.O., S.A., Y.K., and N.S.; by the Four Seasons Ladies Clinic Research Grant; by the Sumitomo Chemical Co. Ltd. Research Grant; by a Grant for the Joint Research Project of the Research Institute for Microbial Diseases, Osaka University to T.K.; and by the Japan Society for the Promotion of Science [grant numbers 17K08889 and 21K07984 to T.K.; 20K18482 to N.K.; 20K17025 to S.A.; 20K16499 to N.S.; 22K20860 to Y.K.; and 20K16028 to S.O.]

Appendix A. Supplementary data

Supplementary data to this article can be found online at https://doi.org/10.1016/j.bbrc.2022.11.088.

References

[1] G.E. White, A.J. Iqbal, D.R. Greaves, D.R. Greaves, CC chemokine receptors and chronic inflammation—therapeutic opportunities and pharmacological challenges, Pharmacol. Rev. 65 (2013) 47–89, https://doi.org/10.1124/pr.111.005074.

[2] F. Liao, R. Alderson, J. Su, S.J. Ullrich, B.L. Kreider, J.M. Farber, STRL22 is a receptor for the CC chemokine MIP-3α, Biochem. Biophys. Res. Commun. 236 (1997) 212–217, https://doi.org/10.1006/bbrc.1997.6936.

[3] M.C. Dieu-Nosjean, A. Vicari, S. Lebecque, C. Caux, Regulation of dendritic cell trafficking: a process that involves the participation of selective chemokines, J. Leukoc. Biol. 66 (1999) 252–262, https://doi.org/10.1002/jlb.66.2.252.

[4] D.L. Rossi, A.P. Vicari, K. Franz-Bacon, T.K. McClanahan, A. Zlotnik, Identification through bioinformatics of two new macrophage proinflammatory human chemokines: MIP-3α and MIP-3β, J. Immunol. 158 (1997) 1033–1036.

[5] K. Hieshima, T. Imai, G. Opdenakker, J. Van Damme, J. Kusuda, H. Tei, Y. Sakaki, K. Takatsuki, R. Miura, O. Yoshie, H. Nomiyama, Molecular cloning of a novel human CC chemokine liver and activation-regulated chemokine (LARC) expressed in liver. Chemotactic activity for lymphocytes and gene localization on chromosome 2, J. Biol. Chem. 272 (1997) 5846–5853, https://doi.org/10.1074/jbc.272.9.5846.

[6] R. Hromas, P.W. Gray, D. Chantry, R. Godiska, M. Krathwohl, K. Fife, G.I. Bell, J. Takeda, S. Aronica, M. Gordon, S. Cooper, H.E. Broxmeyer, M.J. Klemsz, Cloning and characterization of exodus, a novel β-chemokine, Blood 89 (1997) 3315–3322.

[7] G.P. Meares, X. Ma, H. Qin, E.N. Benveniste, Regulation of CCL20 expression in astrocytes by IL-6 and IL-17, Glia 60 (2012) 771–781, https://doi.org/10.1002/glia.22307.

[8] M.M. Guerrini, K. Okamoto, N. Komatsu, S. Sawa, L. Danks, J.M. Penninger, T. Nakashima, H. Takayanagi, Inhibition of the TNF family cytokine RANKL prevents autoimmune inflammation in the central nervous system, Immunity 43 (2015) 1174–1185, https://doi.org/10.1016/j.immuni.2015.10.017.

[9] D.R. Littman, A.Y. Rudensky, Th17 and regulatory T cells in mediating and restraining inflammation, Cell 140 (2010) 845–858, https://doi.org/10.1016/j.cell.2010.02.021.

[10] R. Villares, V. Cadenas, M. Lozano, L. Almonacid, A. Zaballos, C. Martínez-A, R. Varona, CCR6 regulates EAE pathogenesis by controlling regulatory $CD4^+$ T-cell recruitment to target tissues, Eur. J. Immunol. 39 (2009) 1671–1681, https://doi.org/10.1002/eji.200839123.

[11] A. Elhofy, R.W. Depaolo, S.A. Lira, N.W. Lukacs, W.J. Karpus, Mice deficient for CCR6 fail to control chronic experimental autoimmune encephalomyelitis, J. Neuroimmunol. 213 (2009) 91–99, https://doi.org/10.1016/j.jneuroim.2009.05.011.

[12] A. Liston, R.E. Kohler, S. Townley, S. Haylock-Jacobs, I. Comerford, A.C. Caon, J. Webster, J.M. Harrison, J. Swann, I. Clark-Lewis, H. Korner, S.R. McColl, Inhibition of CCR6 function reduces the severity of experimental autoimmune encephalomyelitis via effects on the priming phase of the immune response, J. Immunol. 182 (2009) 3121–3130, https://doi.org/10.4049/jimmunol.0713169.

[13] T. Yamazaki, X.O. Yang, Y. Chung, A. Fukunaga, R. Nurieva, B. Pappu, N. Martin-Orozco, H.S. Kang, L. Ma, A.D. Panopoulos, S. Craig, S.S. Watowich, A.M. Jetten, Q. Tian, C. Dong, CCR6 regulates the migration of inflammatory and regulatory T cells, J. Immunol. 181 (2008) 8391–8401, https://doi.org/10.4049/jimmunol.181.12.8391.

[14] A. Reboldi, C. Coisne, D. Baumjohann, F. Benvenuto, D. Bottinelli, S. Lira, A. Uccelli, A. Lanzavecchia, B. Engelhardt, F. Sallusto, C-C chemokine receptor 6-regulated entry of TH-17 cells into the CNS through the choroid plexus is required for the initiation of EAE, Nat. Immunol. 10 (2009) 514–523, https://doi.org/10.1038/ni.1716.

[15] M. Ohtsuka, M. Sato, H. Miura, S. Takabayashi, M. Matsuyama, T. Koyano, N. Arifin, S. Nakamura, K. Wada, C.B. Gurumurthy, i-GONAD: a robust method for in situ germline genome engineering using CRISPR nucleases, Genome Biol. 19 (2018) 25, https://doi.org/10.1186/s13059-018-1400-x.

[16] K. Tanaka, K. Ichiyama, M. Hashimoto, H. Yoshida, T. Takimoto, G. Takaesu, T. Torisu, T. Hanada, H. Yasukawa, S. Fukuyama, H. Inoue, Y. Nakanishi, T. Kobayashi, A. Yoshimura, Loss of suppressor of cytokine signaling 1 in helper T cells leads to defective Th17 differentiation by enhancing antagonistic effects of IFN-γ on STAT3 and Smads, J. Immunol. 180 (2008) 3746–3756, https://doi.org/10.4049/jimmunol.180.6.3746.

[17] J.N. Lancaster, Y. Li, L.I.R. Ehrlich, Chemokine-mediated choreography of thymocyte development and selection, Trends Immunol. 39 (2018) 86–98, https://doi.org/10.1016/j.it.2017.10.007.

[18] R.E. Kohler, A.C. Caon, D.O. Willenborg, I. Clark-Lewis, S.R. McColl, A role for macrophage inflammatory protein-3α/CC chemokine ligand 20 in immune priming during T cell-mediated inflammation of the central nervous system, J. Immunol. 170 (2003) 6298–6306, https://doi.org/10.4049/jimmunol.170.12.6298.

[19] M.D. Bunting, I. Comerford, E.E. Kara, H. Korner, S.R. McColl, CCR6 supports migration and differentiation of a subset of DN1 early thymocyte progenitors but is not required for thymic nTreg development, Immunol. Cell Biol. 92 (2014) 489–498, https://doi.org/10.1038/icb.2014.14.